

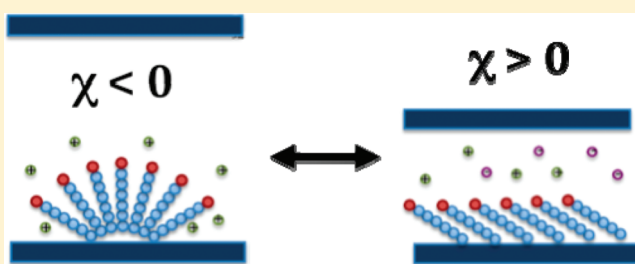
Surfactant Two-Dimensional Self-Assembly under Confinement

Maria L. Sushko* and Jun Liu

Pacific Northwest National Laboratory, Richland, Washington 99352, United States

Supporting Information

ABSTRACT: Confinement-induced structural rearrangements in supported self-assembled surfactant layers in aqueous salt solutions are investigated using classical density functional theory. The systematic study of the influence of the nature of electrolyte revealed that 2:1 electrolyte stabilizes the hemicylindrical configuration of ionic surfactant layers, while a confinement-induced transition to a tilted monolayer configuration was found in symmetric 1:1 and 2:2 electrolytes. On the basis of this study, we formulate a general model for the energetics of structural rearrangements in supported surfactant layers. This model provides a basis for directed self-assembly of surfactant templates with desired structure and stability for scalable synthesis of nanocomposite functional materials, templated crystal growth, and biomolecule adsorption.



1. INTRODUCTION

Organic templates provide a versatile method for the synthesis of nanostructured materials and immobilization of biomolecules. This mechanism is widely used in nature to direct the nucleation and growth of a variety of highly regular structures with unusual properties, such as shells, bone, and teeth. While proteins direct biomineralization, in materials synthesis, the templating role is usually played by supported surfactant layers. The main bottleneck in utilizing this powerful method for practical applications is a lack of fundamental understanding of the main driving forces for surfactant self-assembly at surfaces determining the structure of surfactant layer.^{1,2} Another crucial factor is the stability of the template. It has been shown experimentally and theoretically that the template structure changes during the templated growth of calcium carbonate^{3,4} and self-assembly of multilayer materials.⁵ This effect is the consequence of specific interactions between organic and inorganic phases and of a purely geometrical confinement of the template.

Here, we make an important step toward elucidating the main factors determining the structure and stability of surfactant templates by elucidating the effects of electrolyte and geometrical confinement. Our theoretical approach, based on the classical density functional theory, allows deconvoluting the components of the free energy corresponding to excluded volume and ion correlation effects and surfactant interactions with the surface and the solvent. On the basis of the analysis of the evolution of the individual components of the free energy in response to the changes in external parameters, we were able to formulate a general model for structural rearrangements in surfactant layers. This model can be directly used to control the properties of surfactant templates for hierarchical self-assembly of functional materials and immobilization of biomolecules for a wide range of applications, such as biosensing and energy and data storage to name a few.

First, we briefly review the current theoretical models and experimental data on the properties of surfactant and block copolymers under confinement. Several excellent reviews summarize the current understanding of the physics of self-assembly of block copolymers in thin films.^{6–10} Therefore, we will just outline here the main factors influencing block-copolymer film morphology. Extensive experimental and theoretical research on these systems revealed that the structure of these films depends on the interactions of the blocks with confining walls¹¹ and on the ratio between the film thickness and the characteristic length scale of block copolymers.^{12–14} Another important factor determining the structure of confined block-copolymer solutions is the confining geometry itself. The structures formed under symmetric slit pore confinement are different from those in supported films⁶ or in cylindrical pores.¹⁵ Purely geometrical confinement not only can induce structural changes in block-copolymer solutions, but also can trigger a complete mixing of polymer blends, which are immiscible in bulk solutions, and give rise to a two-dimensional structuring.¹⁶

Although many general conclusions on the driving forces for confinement-induced morphologies of block copolymers are also relevant for the structural properties of confined low molecular weight surfactant systems, there are some important differences. For example, because of significantly lower conformational entropy of surfactant molecules compared to that of high molecular weight block copolymers, some entropy-driven transitions, characteristic to block copolymers, may not occur in surfactant systems. Moreover, because of different entropy–enthalpy balance in surfactant and copolymer solutions, some of the morphologies observed in

Received: January 12, 2011

Revised: February 22, 2011

Published: March 28, 2011

aqueous solutions of block copolymers may only be formed in ternary surfactant/oil/water mixtures.¹⁷

The effect of confinement on the morphology and properties of low molecular weight surfactant films is less studied. Experimental studies revealed two main features of these systems. (1) The cylindrical pore confinement was reported to induce the formation of helical structures of achiral surfactants.¹⁸ (2) Surface force and atomic force microscopy (AFM) measurements demonstrated that monolayers of cationic surfactants undergo structural rearrangements under confinement.¹⁹ When a pre-formed surfactant film was immersed in water, an evolution from a uniform layer to patches of bilayer or hemimicelles was observed. Moreover, the stability of cationic surfactant layers was found to depend on the nature of counterions: CTAF layers were more stable under confinement in surface force experiments than CTAB.¹⁹

The theoretical investigations of confined surfactants are also less abundant compared to the studies of block copolymers.^{20–47} Most surfactant studies were done using different flavors of the mean-field approximation. In particular, self-consistent field calculations for nonionic surfactants in slit pores reveal the confinement-induced symmetry breaking in the system with identical hydrophobic confining surfaces.⁴⁸ The transition is accompanied by the change in sign of the total force acting between two surfactant-coated surfaces. A similar mean-field model has been used to study the confinement effects on the layers of cationic surfactants between two positively charged surfaces in the presence of 1:1 electrolyte.⁴⁹ In these systems at separations larger than the thickness of surfactant layer and at the charge compensation point, the amount of adsorbed surfactant is determined by the electrostatic interactions with the surfaces. However, at shorter separations, when the surfactant layers begin to merge, the system undergoes a phase transition. At these separations, the interactions between surfactant tails play a key role in the structure of surfactant layers and in the exchange between surfactants and co-ions at the surface.⁴⁹ These studies demonstrate a rich behavior of surfactants at surfaces. However, a fundamental understanding of the driving forces for surfactant self-assembly at surfaces and in confined environment has yet to be developed.

To gain new insights into confinement-induced structural rearrangements in surfactant layers, we employ a theoretical method, which is more detailed than the mean-field approaches but which does not extend to the atomistic detail. Nevertheless, the model retains the information on the binding energies between all the components of the system. This compromise between the level of detail and the required accuracy provides a clear physical meaning of all the components of the free energy and, therefore, furnishes a comprehensive model of surfactant system. This feature is not present in atomistic force-field simulations in which interactions are the result of the fitting to a certain functional form and represent a combination of several types of intermolecular forces. We consider an asymmetric situation of the substrate with specific interactions with surfactant blocks and an inert confining wall. Therefore, we study a purely geometrical confinement. The latter is relevant to the problems of supported thin films and of hierarchical self-assembly of multicomponent materials on surfactant film templates.⁵⁰ To gain a better understanding of the driving forces for various structure formation in confined ionic surfactant solutions, we study the effect of the nature and valency of co-ions and counterions.

2. METHODS

We use the classical density functional approach (cDFT) described previously.^{51–53} In this model, the surfactant molecules are constructed as the chains of spherical segments representing surfactant functional groups. Co-ions and counterions in solution are also represented by spherical particles of certain diameter and charge. All calculations were performed for block surfactants of the A₆B type in aqueous electrolyte solutions confined between two flat surfaces. Segments A are neutral and have the diameter of 0.6 nm. The charge and diameter of segments B are -1 and 0.6 nm, respectively. The aqueous salt solution is approximated as a dielectric medium with $\epsilon = 78$ and certain densities of positively and negatively charged spherical particles representing the ions. We considered aqueous NaCl, MgCl₂, CaCl₂, and CaCO₃ solutions. Ionic diameters for the ions used in this study are 0.23 nm for Na⁺, 0.198 nm for Ca²⁺, 0.13 nm for Mg²⁺, 0.36 nm for Cl[−], and 0.532 nm for CO₃^{2−}.⁵⁴

To determine the equilibrium configuration of the system, the total Helmholtz free energy functional is minimized with respect to the densities of all the species. It is convenient to partition the total free energy of the system into so-called ideal (F^{id}) and excess parts (F^{ex}). The ideal free energy corresponds to the free energy of noninteracting surfactant molecules in solution. It is determined by the contributions from surfactant and small ion configurational entropies and surfactant intramolecular bonding potential, $V_b(\vec{R})$. The latter is defined as

$$\exp(-V_b(\vec{R})/kT) = \prod_{i=1}^{M-1} (\delta(|\vec{r}_{i+1} - \vec{r}_i| - \sigma_s)/4\pi\sigma_s^2) \quad (1)$$

where M is the total number of segments in each surfactant molecule and δ is the Dirac delta function. The ideal free energy can be calculated exactly as

$$F^{\text{id}} = kT \int d\vec{R} \rho_M(\vec{R}) [\ln \rho_M(\vec{R}) - 1] + \int d\vec{R} \rho_M(\vec{R}) V_b(\vec{R}) + kT \sum_{\alpha=+, -} \int d\vec{r} \rho_{\alpha}(\vec{r}) [\ln \rho_{\alpha}(\vec{r}) - 1] \quad (2)$$

where $\rho_M(\vec{R})$ is a multidimensional density profile of surfactant segments as a function of surfactant configuration $\vec{R} \equiv (\vec{r}_1, \vec{r}_2, \dots, \vec{r}_M)$ and $\rho_{\alpha}(\vec{r})$ are the density profiles of small ions.

The excess free energy is not known exactly, and certain approximations have to be made. In our model, the hard-sphere repulsion, electrostatic correlation, direct Coulomb, chain connectivity, and segment/segment and segment/surface attraction or repulsion terms have been included in the expression for the excess Helmholtz functional

$$F^{\text{ex}} = F_{\text{hs}}^{\text{ex}} + F_{\text{el}}^{\text{ex}} + F_{\text{C}}^{\text{ex}} + F_{\text{ch}}^{\text{ex}} + F_{\text{att}}^{\text{ex}} \quad (3)$$

The hard-sphere repulsion was calculated using the fundamental measure theory.⁵⁵ The corresponding free energy ($F_{\text{hs}}^{\text{ex}}$) can then be expressed as an integral of the functional of weighted densities ($n_w(\vec{r})$):

$$F_{\text{hs}}^{\text{ex}} = kT \int \Phi^{\text{hs}}[n_w(\vec{r})] d\vec{r} \quad (4)$$

The electrostatic correlation term ($F_{\text{el}}^{\text{ex}}$) can be derived using the mean spherical approximation^{56,57}

$$F_{\text{el}}^{\text{ex}} = F_{\text{el}}^{\text{ex}}[\{\rho_{\alpha}^{\text{bulk}}\}] - kT \int d\vec{r} \sum_{\alpha=+,-} \Delta C_{\alpha}^{(1)\text{el}}(\rho_{\alpha}(\vec{r}) - \rho_{\alpha}^{\text{bulk}}) - \frac{kT}{2} \int \int d\vec{r} d\vec{r}' \sum_{i,j=+,-} \Delta C_{ij}^{(2)\text{el}}(|\vec{r} - \vec{r}'|) (\rho_i(\vec{r}) - \rho_i^{\text{bulk}})(\rho_j(\vec{r}') - \rho_j^{\text{bulk}}) \quad (5)$$

where the first- and second-order direct correlation functions are defined as

$$\Delta C_{\alpha}^{(1)\text{el}} = -\mu_{\alpha}^{\text{el}}/kT \quad (6)$$

$$\Delta C_{ij}^{(2)\text{el}}(|\vec{r} - \vec{r}'|) = \begin{cases} -\frac{q_i q_j e^2}{kT\epsilon} \left[\kappa - 4\kappa^2(|\vec{r} - \vec{r}'|) - \frac{1}{(|\vec{r} - \vec{r}'|)} \right], & (|\vec{r} - \vec{r}'|) \leq \sigma_{ij} \\ 0, & (|\vec{r} - \vec{r}'|) > \sigma_{ij} \end{cases} \quad (7)$$

In these equations, μ_{α}^{el} is the chemical potential of the mobile ions, κ is the inverse Debye length, and $\sigma_{ij} = (\sigma_i + \sigma_j)/2$.

The direct Coulomb term is calculated exactly giving the following free-energy contribution:

$$F_{\text{C}}^{\text{ex}} = \frac{kTl_{\text{B}}}{2} \sum_{i,j=B,+,-} \int \int \frac{q_i q_j \rho_i(\vec{r}) \rho_j(\vec{r}')}{|\vec{r} - \vec{r}'|} d\vec{r} d\vec{r}' \quad (8)$$

where $q_{i(j)}$ are the valences of the charged species and the Bjerrum length is defined as $l_{\text{B}} = [(e^2)/(kT\epsilon)]$.

The formation of bonds between surfactant segments leads to the loss in entropy of the system, which can be expressed using the first-order perturbation theory⁵⁸ as

$$F_{\text{ch}}^{\text{ex}} = kT \frac{1-M}{M} \int n_0 \ln(y(\sigma_i, n_{\omega})) d\vec{r} \quad (9)$$

In this expression, M is the number of segments in the chain. The expression for the contact value of the cavity correlation function, $y(\sigma_i, n_{\omega})$, is given elsewhere.^{59–61}

We use simple square-well potentials to describe the attraction/repulsion interactions between surfactant segments and between the segments and the surface in the form

$$\varphi_{ij}(r) = \begin{cases} \infty, & r < 0 \\ \varepsilon_{ij}, & 0 < r < \sigma_s \\ 0, & r > \gamma\sigma_s \end{cases} \quad (10)$$

$$\varphi_{iw}(r) = \begin{cases} \varepsilon_{iw}, & 0 < r < \sigma_s \\ 0, & \text{otherwise} \end{cases} \quad (11)$$

where indices i, j run over all surfactant monomers, w stands for wall, r is the distance between surfaces of the spheres or between the sphere and the wall, and $\gamma = 1.2$ as in ref 53. The following parameters were used in short-range potentials: $\varepsilon_{\text{AA}} = -1.0$, $\varepsilon_{\text{BB}} = -1.0$, $\varepsilon_{\text{AB}} = 0.5$, $\varepsilon_{\text{AW}} = -0.5$, $\varepsilon_{\text{BW}} = 0.5$. The corresponding

mean-field approximation for the free energy for these non-bonded interactions is then

$$F_{\text{att}}^{\text{ex}} = \frac{1}{2} \int \int d\vec{r} d\vec{r}' \sum_{i,j \in A,B} \rho_i(\vec{r}) \rho_j(\vec{r}') \varphi_{ij}(|\vec{r} - \vec{r}'|) + \int d\vec{r} \sum_{i \in A} \rho_i(\vec{r}) \varphi_{iw}(r) + \int d\vec{r} \sum_{i \in B} \rho_i(\vec{r}) \varphi_{iw}(r) \quad (12)$$

For surfactants at surfaces, the density profiles are only changing in the direction normal to the surface. Therefore, in the following, we will consider a one-dimensional case. We choose the coordinate system with the z -axis normal to the surface with the origin at the surface. Then, the minimization of the grand potential leads to the following set of equations for the density profiles of surfactant segments and small ions:^{53,60}

$$\rho_{\alpha}(z) = \exp \left[\frac{\mu_{\alpha} - \lambda_{\alpha}(z)}{kT} \right] \quad (13)$$

$$\rho_A(z) = \exp \left[\frac{\mu_M}{kT} \right] \sum_{i \in A} G_L^i(z) \exp \left[-\frac{\lambda_i(z)}{kT} \right] G_R^i(z) \quad (14)$$

$$\rho_B(z) = \exp \left[\frac{\mu_M}{kT} \right] \sum_{i \in B} G_L^i(z) \exp \left[-\frac{\lambda_i(z)}{kT} \right] G_R^i(z) \quad (15)$$

where the left and right recurrence functions are calculated as

$$G_L^i(z) = \frac{1}{2\sigma_s} \int_{z-\sigma_s}^{z+\sigma_s} \exp \left[-\frac{\lambda_{i-1}(z)}{kT} \right] G_L^{i-1}(z) dz \quad (16)$$

$$G_R^i(z) = \frac{1}{2\sigma_s} \int_{z-\sigma_s}^{z+\sigma_s} \exp \left[-\frac{\lambda_{i+1}(z)}{kT} \right] G_R^{i+1}(z) dz \quad (17)$$

with $G_L^1(z) = 1$ and $G_R^M(z) = 1$. Index $i = 1, 2, \dots, M$.

In these expressions, the effective field λ_k is defined as

$$\lambda_k(z) = \frac{\partial F^{\text{ex}}}{\partial \rho_k(z)} + \Psi_k(z) \quad (18)$$

where $\Psi_k(z)$ is the external potential. The chemical potential of mobile ions, μ_{ω} in eq 13 is calculated using the overall electroneutrality condition. Equations 13–15 can be solved self-consistently using a Picard iteration method. The output densities were constructed from the input densities using the mixing parameter of 0.005. The convergence was considered to be achieved when the difference between the input and the output density profiles became smaller than 10^{-6} . We used a grid of points along the z -direction equally spaced by the distances of $\sigma_s/10$.

3. RESULTS

3.1. NaCl Solutions. Confining the surfactant layer in 0.01 M NaCl solution between two parallel surfaces results in a gradual transition from hemicylindrical configuration of the surfactant layer to a monolayer of surfactant molecules with either ordered tilted chains of A-segments, as shown in Figure 1, or disordered chains. The transition occurs via a coexistence of both configurations at 10 nm separation of the confining walls (Figure 1c) and results in the change of the average height of surfactant layer from 1.16 nm for a 30 nm pore to 0.7 nm for a 3 nm pore. The

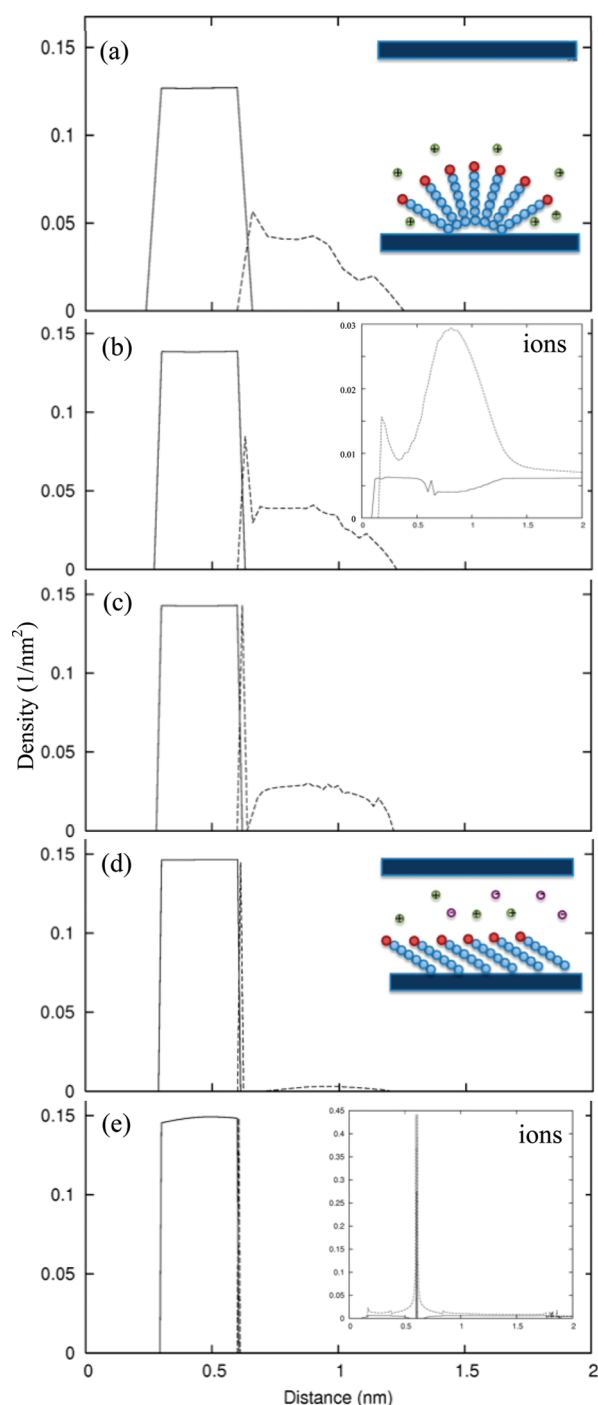


Figure 1. Density profiles of segments A (solid lines) and segments B (dashed lines) for AAAAAAB surfactants in aqueous NaCl solution confined between two flat surfaces separated by the distances of 30 nm (a), 15 nm (b), 10 nm (c), 6 nm (d), and 3 nm (e). The insets to b and e show the corresponding density profiles of co-ions (solid lines) and counterions (dashed lines). The axes' legends for these inserts are the same as in the corresponding main figures. All densities are given with respect to the position of the centers of the spheres representing segments A and B and ions. The schematics for the structure of surfactant layers are given in the insets to a and d. Segments A, B, co-ions, and counterions are represented by the blue, red, purple, and gray spheres, respectively. Both stretched and bent configurations of the A chains in hemicylindrical micelles and in the monolayer can correspond to the observed density distributions.

transition is driven by the changes in the structure of the aqueous salt solution. As the system becomes more confined, the mobile ions are driven closer to the surfactant layer increasing the density in the diffuse layer of counterions around surfactant tail-groups (insets to Figure 1b, e). The increase in the effective counterion density increases the electrostatic attractive force acting on surfactant-charged groups in the direction away from the surface. This leads to the shift of the balance of the attractive/repulsive interactions between surfactant molecules and the surface toward the repulsion inducing the phase transformation in the surfactant layer. Alternatively, this effect can be understood as the decrease in the effective volume of the charged surfactant tail-groups because of the increase in electrostatic screening, which leads to the increase in the critical packing parameter of the system.

The pore width dependence of different components of the free energy of the system exhibits the transitions in the region of 5–10 nm of confining walls. In particular, the Coulomb energy of the charged surfactant tail-groups changes from almost zero for $d > 10$ nm to attractive (Figure 2) reflecting the increase in the normal force acting on surfactants in the direction away from the surface. Simultaneously, the stretching of the chains results in the weakening of the van der Waals attractive forces with the surface facilitating the transition from the hemicylindrical to the monolayer configuration of surfactant layer. Confinement induces the increase in excluded volume effects, which are described by two free energy terms: entropic chain connectivity term ($F_{\text{ch}}^{\text{ex}}$), which describes the indirect interactions due to the excluded volume effects, and enthalpic hard sphere repulsion ($F_{\text{hs}}^{\text{ex}}$). While the confinement-induced entropy loss monotonically increases with the decrease in the distance between the walls, the hard-sphere repulsion does not change while the monolayer remains in the hemicylindrical configuration but increases rapidly with confinement of the system in the monolayer configuration (Figure 2). The latter is due to confinement-induced increase in the tilt angle of the molecules and, therefore, to the decrease in the inter-molecular distances in surfactant layer.

3.2. MgCl_2 and CaCl_2 Solutions. Simulations of surfactant conformation in a slit pore in 2:1 electrolyte show that both MgCl_2 and CaCl_2 stabilize the hemicylindrical configuration (Figure 3). In these solutions, confinement does not induce qualitative changes in the structure of surfactant layer but leads to the decrease in the average hemicylinder height from 1.15 nm for the wide slit pore to 0.75 nm for the narrowest pore considered here.

In these solutions, the doubly charged counterions, which have smaller ionic radii than Na^+ , effectively penetrate into the gaps between the hemicylinders and the surface (Figure 3e, inset) rather than form a dense layer above the charged tail-groups of surfactants. This shifts the total balance of forces in the direction toward the surface and, therefore, stabilizes the hemicylindrical configuration. A certain number of co-ions also penetrate into these gaps, which allows for the increase in the total concentration of counterions at the surface.

We have shown in this study and previously⁶² that the electrostatic interactions between the components of the system along with specific interactions between surfactant segments and the surface largely determine the structure of surfactant layers. Therefore, one can expect similar confinement-induced rearrangements in the surfactant layer in both 2:1 salt solutions. However, the model does not distinguish the specific hydration properties of cations that are determined by their polarizabilities

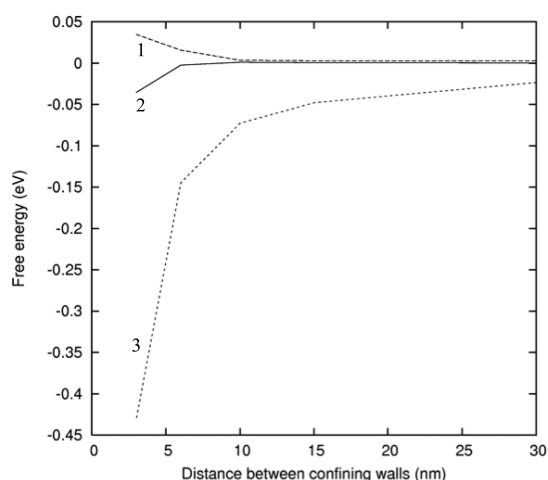


Figure 2. Dependence of the free energy of hard-sphere repulsion (curve 1), Coulomb free energy (curve 2), and the free energy of chain connectivity (curve 3) on the distance between the confining walls.

rather than just by charge densities. Nevertheless, some subtle differences in the density profiles of segments B appear even in this simplified model. In particular, the second peaks for segments B are sharper for the system in CaCl_2 solution compared to MgCl_2 (Figure S1 in the Supporting Information). These differences arise from the difference in the size of counterions. The concentration of larger Ca^{2+} ions in the gaps is smaller, which slightly reduces the force acting on the surfactant head-groups toward the surface, and, therefore, slightly changes the conformation of the surfactant layer.

These differences are also reflected in the dependence of the components of the free energy of the system on the pore width. While the initial confinement makes the Coulomb free energy for the interaction of groups B with each other and the solution more repulsive in both salts, it becomes more attractive in MgCl_2 for small pore sizes and remains almost unchanged in CaCl_2 solutions for pore widths of 3–15 nm (Figure S2 of the Supporting Information).

3.3. CaCO_3 Solutions. The confinement effects are different for the surfactants in the 2:2 electrolyte. Our simulations suggest that confining the anionic surfactant layer in the presence of CaCO_3 first leads to the decrease in the height of surfactant hemicylinders at the surface (Figure 4a, b). The surfactant layer splits into two spatially separated components upon further confinement: the hemicylindrical layer close to the surface and the tilted monolayer approximately 0.7 nm above the surface (Figure 4c). Further decrease in the separation of the confining walls leads to a transition to a uniform monolayer separated from the surface by the layer of mobile cations (Ca^{2+}). In this regime, counterion density has two sharp peaks: one below and one above the monolayer. The upper layer of counterions screens the electrostatic interactions of the charged head-groups of surfactants, while the lower layer compensates for the image interactions across the monolayer and stabilizes the system. In this regime, further confinement induces the increase in the tilt angle of surfactant molecules in the monolayer and the shift of the monolayer closer to the surface, while the qualitative structure of the system remains unchanged (Figure 4d, e).

Although inducing qualitatively different surfactant layer structure, the mechanism of mobile ion redistribution in CaCO_3 solution is very similar to that in MgCl_2 and CaCl_2 solutions. In

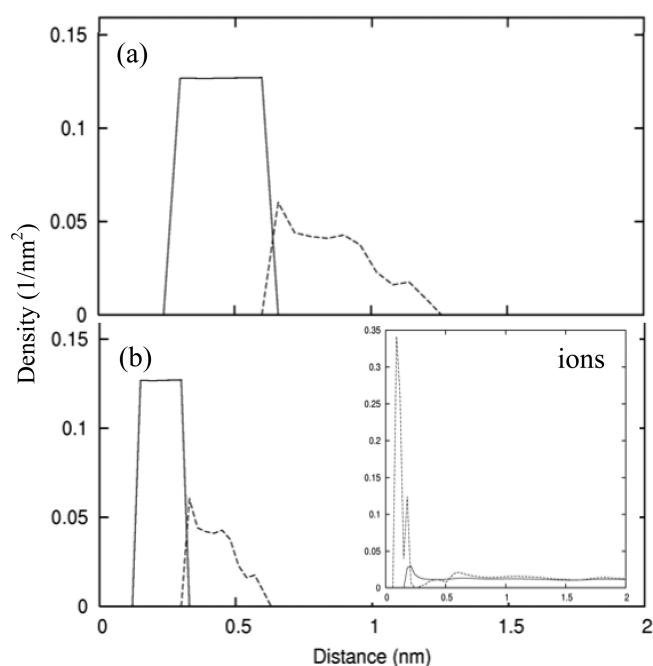


Figure 3. Density profiles of segments A (solid lines) and segments B (dashed lines) for AAAAAAB surfactants in aqueous MgCl_2 solution confined between two flat surfaces separated by the distances of 30 nm (a) and 3 nm (b). The inset to b shows the corresponding density profiles of co-ions (solid lines) and counterions (dashed lines). The axes' legends for the insert are the same as in the corresponding main figures.

this system, counterions are pushed in the gaps between the hemicylinders and the surface (inset to Figure 4e). To compensate for the overpositive charging of this region, a small number of co-ions also diffuse closer to the surface. However, this induces high hard sphere repulsion in the region because of the large size of co-ions. On the other hand, because of the formation of the counterion layer between the surfactant and the surface, the interactions with the surface are substantially weakened. Therefore, it becomes energetically favorable to push the surfactant layer away from the surface. This further reduces the surfactant–surface interactions, which stabilize the hemicylindrical configuration, and facilitates the transition to the monolayer configuration.

4. DISCUSSION

The presented theoretical data allow formulating a general rule governing the structure of self-assembled surfactant layers at surfaces. Following the concepts of the Flory–Huggins type theories for self-assembly in solution,^{63–65} we can introduce an interaction parameter, χ , to quantify the energy balance of interactions acting on surfactant molecules in the direction normal to the surface. Our current study and previous results⁶² suggest that for ionic surfactants at surfaces the main contributions to the corresponding components of the free energy are given by the attractive interactions of surfactant segments with the wall ($F_{\perp}^{\text{att}} = F_{\text{AW}}^{\text{att}} + F_{\text{BW}}^{\text{att}}$, i.e., the sum of the second and third terms in eq 12) and the attraction of charged segments B to co-ions and counterions in solution having predominantly the electrostatic nature ($F_{\perp}^{\text{C}} = F_{\text{BCo}}^{\text{C}} + F_{\text{Bctr}}^{\text{C}}$, eq 8). Defining $\chi = F_{\perp}^{\text{att}} + F_{\perp}^{\text{C}}$ and plotting it as a function of confinement (Figure 5) shows that the change in the sign of the interaction parameter is directly

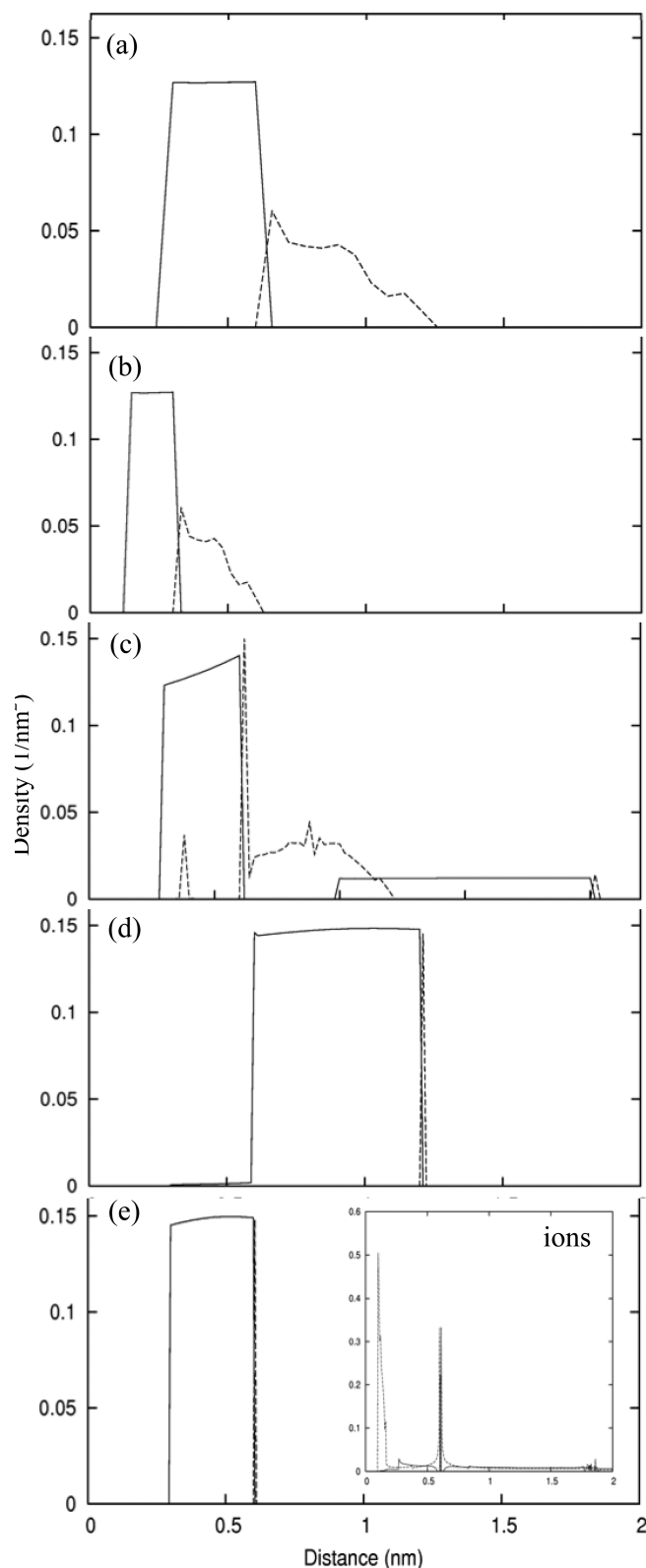


Figure 4. Density profiles of segments A (solid lines) and segments B (dashed lines) for AAAAAAB surfactants in aqueous CaCO_3 solution confined between two flat surfaces separated by the distances of 30 nm (a), 15 nm (b), 10 nm (c), 6 nm (d), and 3 nm (e). The inset to e shows the corresponding density profiles of co-ions (solid lines) and counterions (dashed lines). The axes' legends for the insert are the same as in the corresponding main figures.

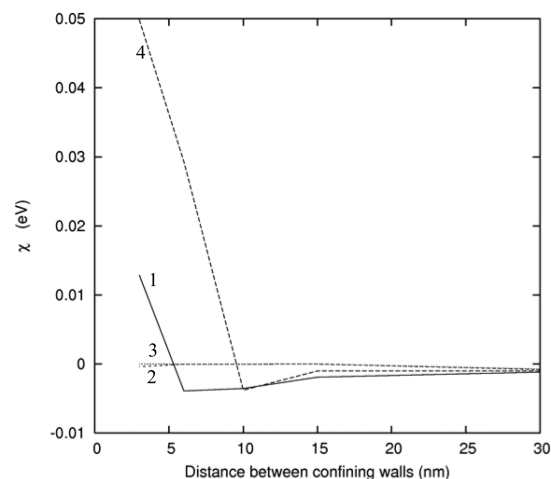


Figure 5. Dependence of the χ parameter on the distance between the confining walls for surfactants in aqueous NaCl (curve 1), MgCl_2 (curve 2), CaCl_2 (curve 3), and CaCO_3 (curve 4) solutions.

correlated with confinement-driven structural rearrangements in surfactant layer. Indeed, when parameter χ is negative, the balance of the normal forces is shifted toward the attraction to the surface and the surfactant layer adopts the hemicylindrical configuration. On the other hand, positive χ induces the monolayer configuration. The same effect has been observed for nonionic surfactants for which the nature of the interactions with the solvent is different. For these systems, the increase in repulsive interactions between blocks B and the surface, leading to the change in sign of the parameter χ , also induced the transition from hemicylinder to the monolayer configuration.⁶²

Although confinement reduces the entropy of the system, our calculations show that the transitions in surfactant layers are enthalpy-driven. The entropic effect is indirect: confinement changes the structure of the aqueous salt solutions which, in turn, strengthens the electrostatic interactions between counterions and surfactant end-groups resulting in the increase in enthalpy. Therefore, it is not possible to separate these two effects.

5. CONCLUSIONS

We presented a classical density functional study of confinement-induced transformations in supported surfactant layers in aqueous salt solutions. The investigation of the influence of different contributions to the free energy of the system on its structure revealed the major role of the normal to the surface interactions. The balance of the interactions between surfactant molecules, the surface, and the solution can be quantified by an interaction parameter χ . In particular, negative values of χ correspond to prevailing surfactant–surface interactions and a hemicylindrical configuration of surfactant layer, while the positive χ corresponds to a tilted monolayer configuration. For example, in 2:1 electrolyte, $\chi < 0$ and surfactant layer remains in a hemicylindrical configuration at all confinements studied, while the change in sign of χ induces the transition in the structure of surfactant layers in 1:1 and 2:2 electrolytes. This model provides a simple tool for choosing the optimum surfactant chemistry and solvent composition for controlled self-assembly of surfactant templates with desired structure and stability. The model can be used to guide specific adsorption of biomolecules and the synthesis of nanostructured functional materials using the self-assembly process.

■ ASSOCIATED CONTENT

S Supporting Information. Density profiles for AAAAAAB surfactants in aqueous MgCl_2 and CaCl_2 solutions (Figure S1) and the dependence of the Coulomb free energy for the interactions of segments B with ions in solution on the distance between the confining walls for these systems (Figure S2). This material is available free of charge via the Internet at <http://pubs.acs.org>.

■ AUTHOR INFORMATION

Corresponding Author

*E-mail: maria.sushko@pnl.gov. Tel.: +1 509 371 7286. Fax: +1 509 371 6242.

■ ACKNOWLEDGMENT

The development of the cDFT software is supported by the Laboratory-Directed Research and Development Program at Pacific Northwest National Laboratory (PNNL). The study of surfactant self-assembly in confined environment is supported by the U.S. Department of Energy, Office of Basic Energy Sciences, Division of Materials Sciences and Engineering under Award KC020105-FWP12152. PNNL is a multiprogram national laboratory operated for DOE by Battelle under Contract DE-AC05-76RL01830.

■ REFERENCES

- Paria, S.; Khilar, K. C. *Adv. Colloid Interface Sci.* **2004**, *110*, 75.
- Atkin, R.; Craig, V. S. J.; Wanless, E. J.; Biggs, S. *Adv. Colloid Interface Sci.* **2003**, *103*, 219.
- Lee, J. R. I.; Han, T. Y. J.; Willey, T. M.; Wang, D.; Meulenberg, R. W.; Nilsson, J.; Dove, P. M.; Terminello, L. J.; van Buuren, T.; De Yoreo, J. J. *J. Am. Chem. Soc.* **2007**, *129*, 10370.
- Duffy, D. M.; Harding, J. H. *Langmuir* **2004**, *20*, 7637.
- Wang, D. H.; Kou, R.; Choi, D.; Yang, Z. G.; Nie, Z. M.; Li, J.; Saraf, L. V.; Hu, D. H.; Zhang, J. G.; Graff, G. L.; Liu, J.; Pope, M. A.; Aksay, I. A. *ACS Nano* **2010**, *4*, 1587.
- Fasolka, M. J.; Mayes, A. M. *Annu. Rev. Mater. Res.* **2001**, *31*, 323.
- Hamley, I. W. *Prog. Polym. Sci.* **2009**, *34*, 1161.
- Kim, J. K.; Lee, J. I.; Lee, D. H. *Macromol. Res.* **2008**, *16*, 267.
- Darling, S. B. *Prog. Polym. Sci.* **2007**, *32*, 1152.
- Balazs, A. C. *Annu. Rev. Phys. Chem.* **2007**, *58*, 211.
- Kellogg, G. J.; Walton, D. G.; Mayes, A. M.; Lambooy, P.; Russell, T. P.; Gallagher, P. D.; Satija, S. K. *Phys. Rev. Lett.* **1996**, *76*, 2503.
- Coulon, G.; Russell, T. P.; Deline, V. R.; Green, P. F. *Macromolecules* **1989**, *22*, 2581.
- Russell, T. P.; Coulon, G.; Deline, V. R.; Miller, D. C. *Macromolecules* **1989**, *22*, 4600.
- Fredrickson, G. H. *Macromolecules* **1987**, *20*, 2535.
- Wu, Y. Y.; Cheng, G. S.; Katsov, K.; Sides, S. W.; Wang, J. F.; Tang, J.; Fredrickson, G. H.; Moskovits, M.; Stucky, G. D. *Nat. Mater.* **2004**, *3*, 816.
- Zhu, S.; Liu, Y.; Rafailovich, M. H.; Sokolov, J.; Gersappe, D.; Winesett, D. A.; Ade, H. *Nature* **1999**, *400*, 49.
- Jain, S.; Bates, F. S. *Science* **2003**, *300*, 460.
- Yang, S.; Zhao, L. Z.; Yu, C. Z.; Zhou, X. F.; Tang, J. W.; Yuan, P.; Chen, D. Y.; Zhao, D. Y. *J. Am. Chem. Soc.* **2006**, *128*, 10460.
- Perkin, S.; Kampf, N.; Klein, J. *J. Phys. Chem. B* **2005**, *109*, 3832.
- Alexander-Katz, A.; Fredrickson, G. H. *Macromolecules* **2007**, *40*, 4075.
- Cao, D. P.; Wu, J. Z. *J. Chem. Phys.* **2005**, *122*, 194703.
- Cao, D. P.; Zhang, X. R.; Wang, W. C. *Appl. Surf. Sci.* **2009**, *255*, 5775.
- Chen, P.; He, X. H.; Liang, H. J. *J. Chem. Phys.* **2006**, *124*, 104906.
- Chen, P.; Liang, H. J. *J. Phys. Chem. B* **2006**, *110*, 18212.
- Feng, J.; Liu, H. L.; Hu, Y. *Macromol. Theory Simul.* **2006**, *15*, 674.
- Feng, J.; Ruckenstein, E. *Polymer* **2002**, *43*, 5775.
- Frischknecht, A. L.; Curro, J. G.; Frink, L. J. D. *J. Chem. Phys.* **2002**, *117*, 10398.
- Han, Y. Y.; Cui, J.; Jiang, W. *Macromolecules* **2008**, *41*, 6239.
- Jain, S.; Chapman, W. G. *Mol. Phys.* **2009**, *107*, 1.
- Lee, J. Y.; Shou, Z.; Balazs, A. C. *Phys. Rev. Lett.* **2003**, *91*, 136103.
- Lee, J. Y.; Shou, Z. Y.; Balazs, A. C. *Macromolecules* **2003**, *36*, 7730.
- Li, S. B.; Chen, P.; Wang, X. H.; Zhang, L. X.; Liang, H. J. *J. Chem. Phys.* **2009**, *130*, 014902.
- Li, S. B.; Wang, X. H.; Zhang, L. X.; Liang, H. J.; Chen, P. *Polymer* **2009**, *50*, 5149.
- Ludwigs, S.; Krausch, G.; Magerle, R.; Zvelindovsky, A. V.; Sevink, G. J. A. *Macromolecules* **2005**, *38*, 1859.
- Miao, B.; Yan, D. D.; Wickham, R. A.; Shi, A. C. *Polymer* **2007**, *48*, 4278.
- Nie, Z. H.; Su, Z. H.; Sun, Z. Y.; Shi, T. F.; An, L. J. *Macromol. Theory Simul.* **2005**, *14*, 463.
- Pinna, M.; Guo, X. H.; Zvelindovsky, A. V. *J. Chem. Phys.* **2009**, *131*, 214902.
- Podariu, I.; Chakrabarti, A. *J. Chem. Phys.* **2003**, *118*, 11249.
- Potemkin, I. I.; Busch, P.; Smilgies, D. M.; Posselt, D.; Papadakis, C. M. *Macromol. Rapid Commun.* **2007**, *28*, 579.
- Rasmussen, K. O. *J. Polym. Sci., Part B: Polym. Phys.* **2004**, *42*, 3695.
- Sivaniah, E.; Hayashi, Y.; Matsubara, S.; Kiyono, S.; Hashimoto, T.; Kukunaga, K.; Kramer, E. J.; Mates, T. *Macromolecules* **2005**, *38*, 1837.
- Tasinkevych, M.; Ciach, A. *Phys. Rev. E* **2005**, *72*, 061704.
- Tsori, Y.; Andelman, D. *J. Polym. Sci., Part B: Polym. Phys.* **2006**, *44*, 2725.
- Wang, Q. *Macromol. Theory Simul.* **2005**, *14*, 96.
- Xiang, H.; Shin, K.; Kim, T.; Moon, S. I.; McCarthy, T. J.; Russell, T. P. *Macromolecules* **2005**, *38*, 1055.
- Xiang, H. Q.; Shin, K.; Kim, T.; Moon, S. I.; McCarthy, T. J.; Russell, T. P. *Macromolecules* **2004**, *37*, 5660.
- Xiao, X. Q.; Huang, Y. M.; Liu, H. L.; Hu, Y. *Macromol. Theory Simul.* **2007**, *16*, 732.
- Leermakers, F. A. M.; Koopal, L. K.; Goloub, T. P.; Vermeer, A. W. P.; Kijlstra, J. *J. Phys. Chem. B* **2006**, *110*, 8756.
- Lokar, W. J.; Koopal, L. K.; Leermakers, F. A. M.; Ducker, W. A. *J. Phys. Chem. B* **2004**, *108*, 15033.
- Wang, D. H.; Choi, D. W.; Li, J.; Yang, Z. G.; Nie, Z. M.; Kou, R.; Hu, D. H.; Wang, C. M.; Saraf, L. V.; Zhang, J. G.; Aksay, I. A.; Liu, J. *ACS Nano* **2009**, *3*, 907.
- Sushko, M. L.; Liu, J. *J. Phys. Chem. B* **2010**, *114*, 3847.
- Wu, J. Z.; Li, Z. D. *Annu. Rev. Phys. Chem.* **2007**, *58*, 85.
- Cao, D. P.; Wu, J. Z. *Macromolecules* **2005**, *38*, 971.
- Nightingale, E. R. *J. Phys. Chem.* **1959**, *63*, 1381.
- Yu, Y. X.; Wu, J. Z. *J. Chem. Phys.* **2002**, *117*, 10156.
- Blum, L. *Mol. Phys.* **1975**, *30*, 1529.
- Hoye, J. S.; Blum, L. *Mol. Phys.* **1978**, *35*, 299.
- Yu, Y. X.; Wu, J. Z. *J. Chem. Phys.* **2002**, *117*, 2368.
- Jiang, J. W.; Liu, H. L.; Hu, Y.; Prausnitz, J. M. *J. Chem. Phys.* **1998**, *108*, 780.
- Jiang, T.; Li, Z. D.; Wu, J. Z. *Macromolecules* **2007**, *40*, 334.
- Jiang, J. W.; Blum, L.; Bernard, O.; Prausnitz, J. M. *Mol. Phys.* **2001**, *99*, 1121.
- Sushko, M. L.; Liu, J. *J. Phys. Chem. B* **2010**, *114*, 3847.
- Dudowicz, J.; Douglas, J. F.; Freed, K. F. *J. Phys. Chem. B* **2008**, *112*, 16193.
- Voets, I. K.; Leermakers, F. A. M. *Phys. Rev. E* **2008**, *78*, 061801.
- Douglas, J. F.; Dudowicz, J.; Freed, K. F. *Phys. Rev. Lett.* **2009**, *103*, 135701.